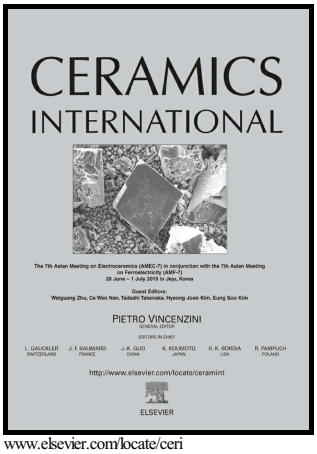

www.elsevier.com/locate/ceri

Effects of fe addition on the mechanical and thermo-mechanical properties of SiC/$FeSi_2$/si composites produced via reactive infiltration

A. Camarano, M. Caccia, J.M. Molina, J. Narciso

PII: S0272-8842(16)30344-3
DOI: http://dx.doi.org/10.1016/j.ceramint.2016.03.196
Reference: CERI12567

To appear in: *Ceramics International*

Received date: 2 February 2016
Revised date: 24 March 2016
Accepted date: 25 March 2016

Cite this article as: A. Camarano, M. Caccia, J.M. Molina and J. Narciso, Effect of fe addition on the mechanical and thermo-mechanical properties o SiC/$FeSi_2$/si composites produced via reactive infiltration, *Ceramic International,* http://dx.doi.org/10.1016/j.ceramint.2016.03.196

Effects of Fe addition on the mechanical and thermo-mechanical properties of $SiC/FeSi_2/Si$ composites produced via reactive infiltration

A. Camarano, M. Caccia, J.M. Molina, J. Narciso

Instituto Universitario de Materiales de Alicante (IUMA), Universidad de Alicante, Apdo. 99, 03080 Alicante, Spain

Author to whom correspondence should be addressed: Mario Caccia, marioraul@ua.es, tel. +34 965 90 93 50

ABSTRACT: Remaining silicon in SiC-based materials produced via reactive infiltration limits their use in high-temperature applications due to the poor mechanical properties of silicon: low fracture toughness, extreme fragility and creep phenomena above 1000ºC. In this paper SiC-FeSi2 composites are fabricated by reactive infiltration of Si-Fe alloys into porous Cf/C preforms. The resulting materials are SiC/FeSi2 composites, in which remaining silicon is reduced by formation of FeSi2. For the richest Fe alloys (35 wt.% Fe) a nominal residual silicon content below 1% has been observed. However this, the relatively poor mechanical properties (bending strength) measured for those resulting materials can be explained by the thermal mismatch of FeSi2 and SiC, which weakens the interface and does even generate new porosity, associated with a debonding phenomenon between the two phases.

KEYWORDS: SiC, composites, CTE, bending strength, Fe-Si

1. INTRODUCTION

With the development of faster and more powerful vehicles arises the challenge of producing more efficient and capable braking technologies. The security requirements for braking procedures, i.e. minimum braking distance or maximum deceleration, in planes, trains or automobiles demand the use of novel materials. Classical brake disks, made of cast irons with variable carbon contents [1-4] are no longer useful for ultimate applications, since their high density and use-induced microstructural transformations [5-7] severely shorten their lifetime. Carbon-carbon composites (C/C) have been widely used as an alternative for high wear applications such as brake discs for their excellent thermal properties, their low density, and their sufficient mechanical properties [8-10]. However, a downside of these materials is their high reactivity with oxygen, which causes the material to get burned slowly. Metal/ceramic composites such as Aluminium/SiC or Aluminium/Al_2O_3 [11] have proven to be adequate for these applications; however their performance/cost ratio is inferior to other composite materials such as C_f/SiC. The latter presents an outstanding resistance to oxidation while maintaining an excellent thermal conductivity, low thermal expansion coefficient, low density and good mechanical properties. Cf/SiC composites are usually prepared by reactive infiltration, which consists of infiltrating molten Si into a C_f/C porous preform [12,13]. As Si infiltrates the preform it reacts with the carbon to form a dense SiC matrix. The main advantage of this synthesis route is that the conditions applied are less

severe than the ones applied in classical sintering techniques of SiC powder, and also that the production time is significantly decreased. Nevertheless, it is essential to work under optimal infiltration conditions [14, 15], and thus it is necessary to identify the effect of the most influent parameters, which are reaction temperature, and infiltration time. The main disadvantage of reactive infiltration as production method is that the materials produced have at least 10% of unreacted Si in their microstructure [16,17]. Si is a very brittle material with poor mechanical properties that limits the performance of the composite. However, it is possible to partially replace this Si phase with a metal silicide phase (Me_xSi_y) by infiltrating the preform with a Si-rich Si-Me alloy [18-21]. By selecting a metal that forms a silicide with better mechanical properties than Si, the performance of the final material can be improved. In order to ensure the viability of infiltrating with a certain Si-Me alloy, it is necessary to perform a wetting study of the alloy on a carbon substrate to determine whether the infiltrating alloy wets the carbon through the proper formation of a SiC interface. This will ensure that the alloy will spontaneously infiltrate a porous carbon preform [18,22-25]. Iron (Fe) forms a Si-rich silicide ($FeSi_2$) with higher fracture toughness than Si and it does not form a stable carbide in the presence of Si, making it an ideal candidate to be used as a replacement for the Si phase in these kind of composite materials [26-29]. Furthermore, it has been reported that several FeSi alloy compositions wet and infiltrate carbon materials while forming a SiC interface [30-31].

In this work, the effect of Fe addition in the microstructure and thermo-mechanical properties of SiC/Si composites was investigated by producing SiC/Si/$FeSi_2$ composites via reactive infiltration with Fe-Si alloys. The mechanical and the thermo-mechanical properties of the composites, and their relationship to the microstructure were studied.

2. EXPERIMENTAL

2.1 Carbon porous preforms

The porous carbon preforms used in this work were kindly supplied by Schunk Graphite Technology. They consist of a mixture of graphitized short carbon fiber and a binder. The density of the preforms varies in the range 0.67-0.87 g/cm^3, with an average total open porosity of 47%. The mean pore diameter is 30 μm.

2.2 Si-Fe alloys

Alloys were in-house prepared in a high-temperature induction furnace by mixing pure Fe (Goodfellow, 99.95% purity) and pure Si (Petroceramics, 99.999% purity). For the purpose of the present work four nominal Si-Fe alloy compositions were selected: Si-5wt.%Fe, Si-15wt.%Fe, Si-25wt.%Fe and Si-35wt%Fe. For each composition the components were pre-melted in a graphite crucible previously coated with boron nitride (BN), under Ar atmosphere (P=0.15 MPa). After the melting temperature was reached, it was maintained for 20 minutes in order to achieve thermal stabilization. Exact alloy compositions and corresponding microstructures were determined by using X-Ray fluorescence (XRF) and optical microscopy (OM), respectively. No traces of BN were

found in the alloys. A more detailed description of the alloy preparation and characterization, as well as the alloys exact composition is provided in Annex A.

2.3 Reactive infiltration

Infiltration of the samples was carried out in a horizontal resistance furnace with an alumina tube under Ar flow of 100 cm^3/min. Carbon preforms of 40x8x4 mm were cut and placed inside an alumina boat-shaped crucible previously coated with BN to prevent reactivity between crucible and excess Si. To reduce oxygen partial pressure inside the tube, a bed of sacrificial char was placed below the samples. Between sample and the sacrificial char, a BN-coated carbon cloth was placed to retain the excess Si and prevent it from reacting with the char. Si and Si-Fe alloys were placed on top of the carbon preform and a SiC cloth was placed between them to act as filter and retain oxides. This procedure allows obtaining clean samples with no adherence to excess Si or surface oxides. The relative position of all components is schematized in Fig. 1.

Before producing the SiC/Si/$FeSi_2$ composite materials, the parameters of reaction temperature and infiltration time were optimized for these preforms using pure Si. For this purpose, infiltrations at three different temperatures (1450, 1500 and 1550 ºC) with three different holding times (3, 5 and 8 h) were performed. For all experiments the heating rate used was 3 º/min. The optimal conditions were established as those for which the highest material density (lowest residual porosity) was obtained. The optimal conditions were then applied to the infiltration with Si-Fe alloys.

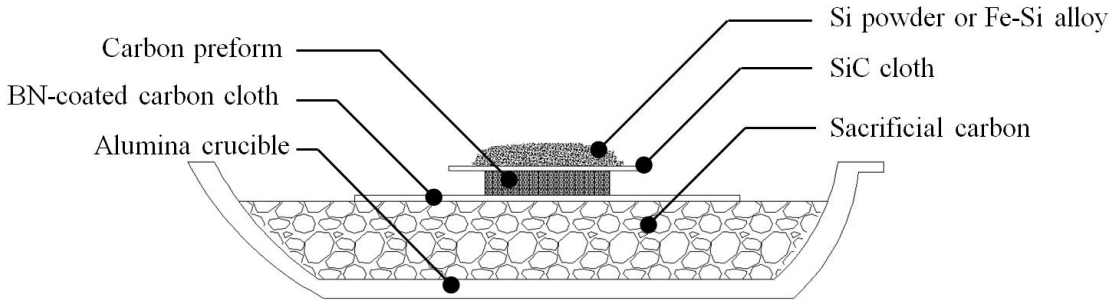

Fig. 1 *Schematized situation of the different components used for infiltration of the preforms*

2.4 Microstructural characterization

Composites microstructures were evaluated using an optical microscope. Samples were polished using standard metallographic techniques (SiC paper until P1200, diamond paste until 1 micron and 0.1 micron coloidal silica). Phases were identified by X-Ray diffraction (XRD) recorded on a Brucker D8-Advanced diffractometer with a Goebel mirror and a Kristalloflex K 760-80 F X-Ray generation system, fitted with a Cu

cathode and a Ni filter. Spectra were registered between 20-80º with a step of 0.1º and a velocity of 2º/min. Pore size distribution and average pore size were obtained with mercury intrusion porosimetry using a Quantachrome Poremaster-60 porosimeter working between 6 and 400 000 kPa.

2.5 Mechanical and thermo-mechanical characterization

The flexural strength of the resulting materials was measured using the three-point-bending test with a span of 32 mm and a crosshead speed of 0.1 mm/min. Prior to bending tests, the surface of all samples was mirror polished using SiC paper and diamond paste up to 1 micron grain size. Thermal expansion coefficient (CTE) were derived from thermal response obtained using a thermo-mechanical analyzer (TMA 2940, TA Instruments). Thermal response curves were obtained by applying a 0.05 N force to the samples under nitrogen atmosphere in the temperature range of 25-900 ºC. Samples were subjected to at least 3 heating and cooling cycles to remove any large residual stress that may have been developed during the processing of the composite.

3. RESULTS AND DISCUSSION

3.1 Carbon preform characterization

Graphite preforms are composed of a graphitized mixture of short carbon fiber and a binder, as it is evidenced in the X-ray diffractogram showed in Fig. 2a. The XRD signal has been deconvoluted for the 2 main diffraction peaks to clearly show the contribution of each type of carbon to the signal. Fig. 2b shows an optical microscopy image of a cross-section of a preform. The light gray phase represents carbon, while the dark gray phase represents pores filled with epoxy resin used to obtain a better contrast with the carbon phase. Carbon fibers with different orientations are observed, and the binder material is found surrounding the fibers. The porosity has no particular geometry and is heterogeneously distributed over the preform. Mercury porosimetry showed that the average pore width is between 20-40 μm, with the presence of smaller porosity with a pore width around 3-4 μm.

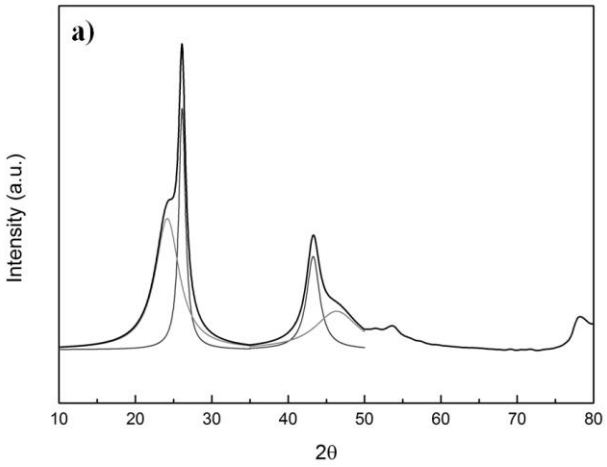

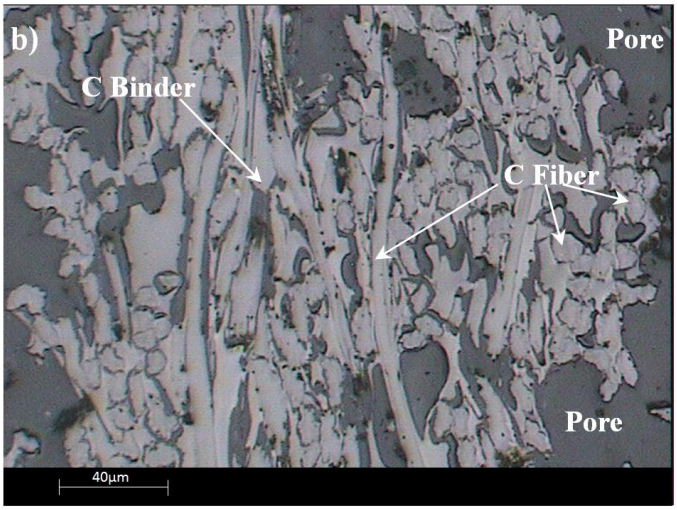

Fig. 2a. X-ray diffractogram of an as received sample. All diffraction peaks correspond to graphite, and the contribution of the different carbon materials has been deconvoluted. 2b. Optical microscopy image of a cross-section of the as received carbon preformed used in the present work.

3.2 Optimization of the infiltration process

Before producing the composite materials, the parameters of infiltration, namely temperature and dwell time, were optimized for the preform used. For this purpose infiltrations with pure Si were performed by using a combination of 3 temperatures and 3 dwell times. The mechanism proposed by Eustathopoulos et al. to explain reactive wetting and infiltration of Si and Si-Me alloys on porous and non-porous carbon materials, respectively, suggests that the infiltration velocity (U_{inf}) at a given temperature is equal or at least of the same order of magnitude than the spreading velocity (U_{spr}) [22,32]. Several wetting studies of Si-Me (Me=Cu, Ni, Co, Al) on carbon substrates have reported that, as predicted by the aforementioned mechanism, the influence of alloy composition on U_{spr} is very weak [19, 33-35], and thus, U_{inf} can be assumed as independent of the alloy composition for Si-rich alloys. Therefore, it is reasonable to assume that the optimal conditions obtained for the infiltrations performed with pure Si are the same as for infiltrations performed with Si-rich Fe-Si alloys. To minimize the effect of the heterogeneous distribution of the porosity inside the preform, and to evaluate the degree of infiltration, the density of the infiltrated sample (ρ_{inf}) was normalized with the density of the original carbon prefom (ρ_{carb}). Fig. 3 shows the values of ρ_{inf}/ρ_{carb} obtained for the different experimental conditions. The highest density values for the infiltrated sample were achieved for the lowest temperature and dwell times. The work of Greil et al. [36] infiltrating carbon preforms obtained from pyrolized wood showed that pores larger than 30 µm remain unfilled after infiltration, while pores with sizes smaller than 30 µm were completely filled with Si. The same phenomenon was observed by Amirthan et al. [37] when infiltrating cotton fabric derived porous preforms. Due to presence of pores between 20-40 µm in the porous preform, capillary forces fail to retain Si in such pores and for increasing dwell time unreacted Si flows through and out of the preform, leaving larger pores partially

unfilled. Infiltration with increasing temperature has indirectly longer dwell times because with the slow heating rates used, it takes longer to reach maximum temperature In fact, a common technique for removal of Si from the SiC/Si material is to heat at higher temperature than infiltration temperature and to maintain this temperature for more than 60 minutes [38,39].

In the light of these results, the optimal infiltration conditions for this carbon preform were selected as 1450 ºC with a dwell time of 3 h.

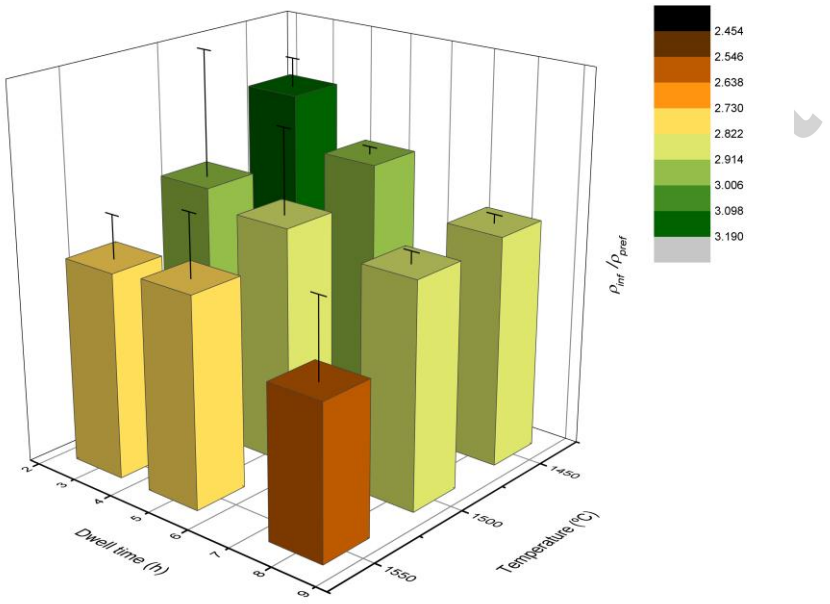

Fig. 3. Values of ρ_{inf}/ρ_{carb} obtained for infiltrations with pure Si. Bars and error bars indicate the mean value and standard deviation respectively. For each set of temperature and dwell time, 4 preforms were manufactured.

3.3 Microstructure of the SiC/Si/$FeSi_2$ composite materials

Fig. 4 shows optical microscopy images of cross-sections of the different composite materials obtained. SiC is depicted in two different dark brown tonalities, Si in grey and $FeSi_2$ in light brown. The different colors observed for SiC are due to the different types of carbon precursors originally present in the preform, i.e. carbon fibers and carbonized binder.

The final microstructure of the composites mimics the microstructure of the carbon preform with scattered porosity filled with the alloy and the generated SiC replacing the original C. No presence of unreacted C or of Fe_3C is found in any of the materials produced. The presence of SiC, Si and $FeSi_2$ is observed in all composites, except for

the one produced with an alloy with 35 wt.% of Fe (Fig. 4g-h) in which the only phases observed are almost exclusively SiC and $FeSi_2$. In this material, the presence of small porosity situated mainly at the SiC/$FeSi_2$ interface is noticed, indicating that there is a debonding of both phases.

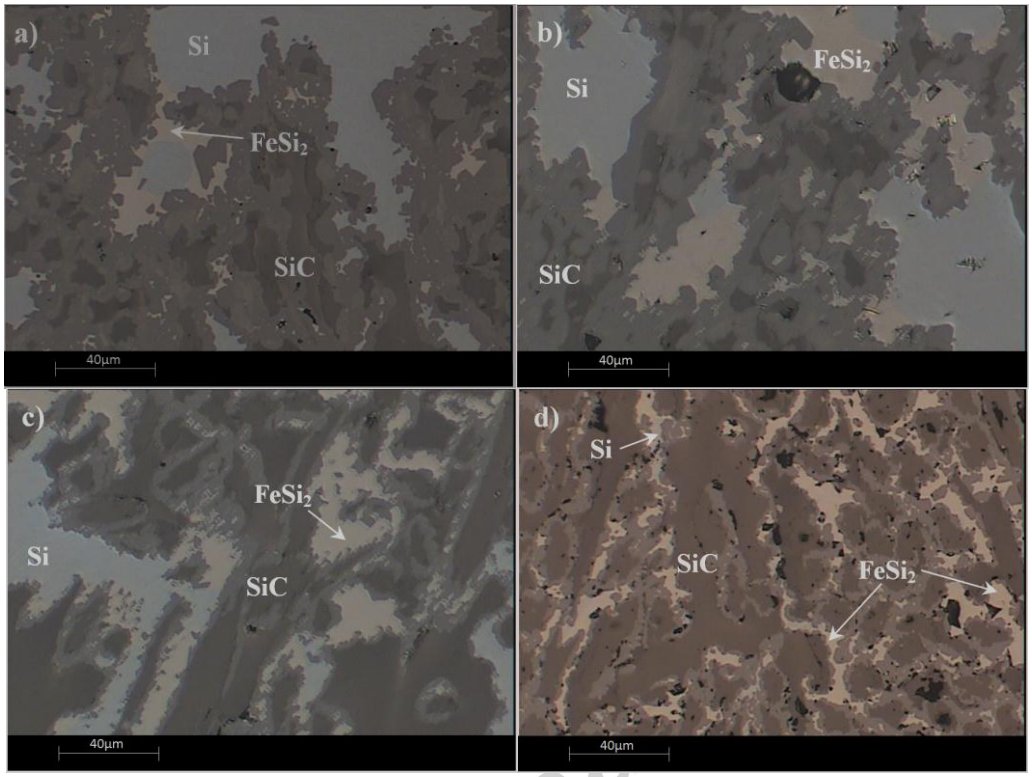

Fig. 4. Optical microscopy images of cross-sections of composites produced with alloys with a Fe content of 5 wt.% (a), 15 wt.% (b), 25 wt.% (c) and 35 wt.% (d).

3.4 Mechanical and thermo-mechanical properties of the SiC/Si/$FeSi_2$ composite materials

Fig. 5 shows the results of the bending tests performed on the composite materials. It becomes almost clear that contents of Fe higher than 5 wt.% in the infiltrating alloy result in a decay in the bending strength (BS) of the composite. Nevertheless the results of BS obtained for the samples prepared with an addition of 5 wt.% Fe showed for some samples an increase in BS and for others a decrease in it. The average value shows a similar result than the ones obtained with pure Si. However due to the large dispersion of the results, consequence of the heterogeneous microstructure in the carbon preform, it is not clear whether this content in Fe favours or not the mechanical resistance of the composite. It would be necessary to carry out an investigation for Fe contents between 0-5 wt.% to attain a better understanding. Since during infiltration porosity of the preform is filled with Si-Fe alloy, samples with higher porosity (lower content in SiC) will present lower BS values than the ones with lower porosity (higher content in SiC).

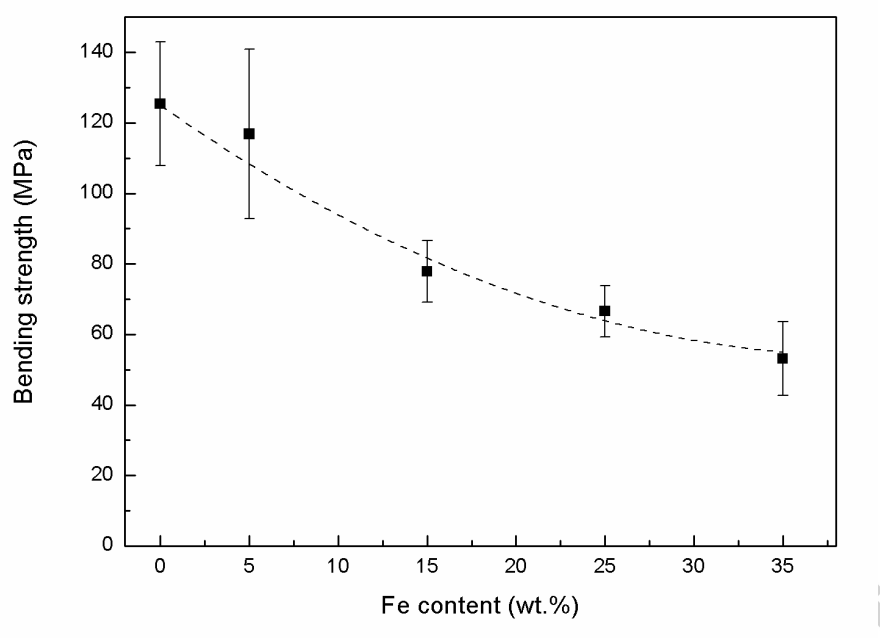

Fig. 5. Bending strength of the composite materials produced. Points and bars indicate the mean value and the standard deviation respectively.

Materials produced with alloys with increasing Fe content also showed decreasing values of final density, indicating that either porosity of the preform remains unfilled after infiltration, or that new porosity is being generated during infiltration. The microstructure analysis performed by OM shows that the original pores are completely filled with alloy in all the samples, suggesting that new porosity is being formed during the synthesis. This phenomenon can be explained by analyzing the CTE values measured for the different composites. The CTE was measured in the range of temperatures of 25-900 ºC and an average value was calculated for that range as shown in Fig. 6. CTE of the composites grows proportionally to the Fe content and reaches a value for the highest content in Fe that doubles the CTE of the SiC/Si composite. The averaged CTE of β-SiC for the same range of temperature is $3.4x10^{-6}$ K^{-1}, so as a result of the thermal incompatibility, in samples with greater content of Fe, there is a de-bonding of the SiC and $FeSi_2$ phases, generating small cracks associated to the SiC/$FeSi_2$ interface. This effect becomes especially relevant for the sample obtained with an alloy with 35 wt.% of Fe, in which SiC and $FeSi_2$ were almost the only phases found. Zhu et al. [31] observed that for composites of FeSi/$FeSi_2$ reinforced with SiC particles, there was a considerable rise in microcrack generation, and they concluded that it was a consequence of the thermal mismatch between the three phases. By XRD they estimated the strain in all phases and observed that $FeSi_2$ presented the highest value of residual strain. Further evidence of this phenomenon is obtained when analyzing the thermal strain response curve (see Fig. 7). Materials produced with pure Si or alloys with Fe contents between 5-25 wt.% show no hysteresis in the thermal strain curve upon cycling. However, the composite material produced with an alloy with 35 wt.% of Fe shows an initial hysteresis that grows with the next 2 cycles, and then is reduced until it disappears with the successive cycles. Hysteresis in the thermal strain

curve is associated to residual stress in the material [40]. The fact that hysteresis appears upon cycling is an additional evidence of the thermal incompatibility between SiC and $FeSi_2$. Due to the brittleness of these composites, when this residual stress surpasses tensile strength of the interface, it generates a crack along it, as observed in the micrographs (see Fig. 4g-h). This phenomenon was observed by Etter et al. [41] for graphite/Aluminum composites as well. In their work they followed crack formation upon cycling using X-Ray tomography.

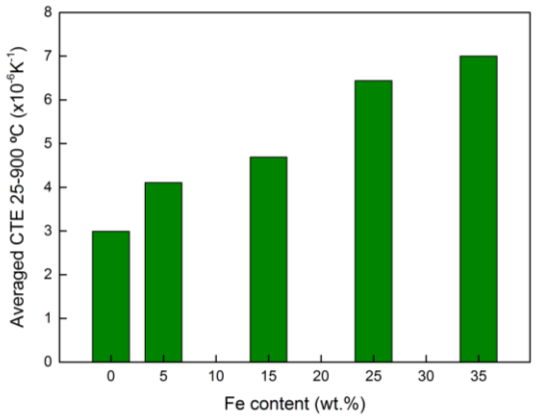

Fig. 6. CTE as a function of Fe content in the infiltrating alloy for the composite materials produced.

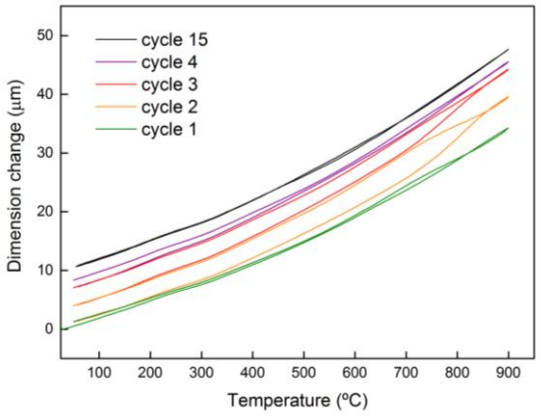

Fig. 7. Thermal strain response curve for the sample produced with an alloy with 35 wt.% Fe.

4. CONCLUSIONS

$SiC/Si/FeSi_2$ composite materials were successfully obtained using the reactive infiltration technique. The microstructure of the composites produced mimics the one of the carbon preform, and a good control of alloy composition was achieved by infiltrating with excess alloy.

Mechanical and thermo-mechanical characterization of the composites showed that additions of Fe greater than 5 wt.% reduced the mechanical performance of the material because of the thermal incompatibility of the $SiC/FeSi_2$ interface. Additions of 5 wt.%

seem to increase mechanical performance of the composite, however the heterogeneity of the preform makes the bending strength data very scattered. CTE measurements showed that additions of 5-15 wt.% of Fe do not increase the overall CTE substantially, while additions greater than 15 wt.% double its value. Microcrack formation was observed for the sample produced with the alloy with 35 wt.% Fe due to the thermal incompatibility between SiC and $FeSi_2$.

ACKNOWLEDGEMENTS

Authors would like acknowledge the financial support received from the Generalitat Valenciana (PROMETEO II/2014/004-FEDER, PhD grant Vali+d and Santiago Grisolia program, GRISOLIA/2013/023), and the European Union's Seventh Framework Programme (FP7/2007-2013) under the HELM project, grant agreement no. 280464 are greatfully acknowledged.

REFERENCES

[1] S. Paniera, P. Dufrénoy, D. Weichertc, An experimental investigation of hot spots in railway disc brakes, Wear 256 (2004) 764-773.
[2] F. Bagnoli, F. Dolce, M. Bernabei, Thermal fatigue cracks of fire fighting vehicles gray iron brake discs, Eng. Fail. Anal. 16 (2009) 152–163.
[3] Lars Hammerström, Staffan Jacobson, Surface modification of brake discs to reduce squeal problems, Wear 261 (2006) 53-57.
[4] H. Sakamoto, K. Hirakawa, Fracture Analysis and Material Improvement of Brake Discs, Inter. J. Series A Sol. Mech. Mat. Eng. 48 (2005) No. 4 Special Issue on Recent Advances in Materials and Processing 458-464.
[5] A.J. Day, M. Tiovic, T.P. Newcomb, Thermal effects and pressure distributions in brakes, P. IMech. Eng., Part D: J. Automo. Eng. 205(3) 199-205.
[6] S. Rhee, R. DuCharme, W. Spurgeon, Characterization of Cast Iron Friction Surfaces, SAE Technical Paper (No. 720056).
[7] W. Österle, I. Dörfel, C. Prietzel, H. Rooch, A.L. Cristol-Bulthé, G. Degallaix, Y. Desplanques, A comprehensive microscopic study of third body formation at the interface between a brake pad and brake disc during the final stage of a pin-on-disc test, Wear 267 (2009) 781-788.
[8] C. Blanco, J. Bermejo, H. Marsh, R. Menendez, Chemical and physical properties of carbon as related to brake performance, Wear 213 (1997) 1-12.
[9] H. Marsh, F. Rodriguez-Reinoso, Science of carbon materials, 1st edition, Publicaciones de la Universidad de Alicante, 2000.
[10] H. Marsh, E. Heintz, F. Rodríguez-Reinoso, Introduction to carbon technologies, 1st edition, Publicaciones de la Universidad de Alicante, 1997.
[11] C. García-Cordovilla, J. Narciso, E. Louis, Abrasive wear resistance of aluminium alloy/ceramic particulate composites, Wear 192 (1996) 170-177.
[12] M. Caccia, J. Narciso, SiC Manufacture via reactive infiltration in: Processing and Properties of Advanced Ceramics and Composites VI: Ceramic Transactions 249, 15-25.
[13] G. Bianchi, P. Vavassori, B. Vila, G. Annino, M. Nagliati, M. Mallah, S. Gianellaf, M. Valle, M. Orlandi, A. Ortona, Reactive silicon infiltration of carbon bonded preforms embedded in powder field modifiers heated by microwaves, Ceram. Inter. 41 (2015) 12439-12446.

[14] N. R. Calderon, M. Martinez-Escandell, J. Narciso, F. Rodriguez-Reinoso, Manufacture of biomorphic SiC components with homogeneous properties from sawdust by reactive infiltration with liquid silicon, J. Amer. Ceram. Soc. 93 (4) (2010) 1003-1009.
[15] N. R. Calderon, M. Martinez-Escandell, J. Narciso, F. Rodriguez-Reinoso, The role of carbon biotemplate density in mechanical properties of biomorphic SiC, J. Europ. Ceram. Soc. 29 (3), (2009) 465-472.
[16] M.N Rahaman, Ceramic Processing and Sintering, 2nd edition, CRC Press, New York, 2003.
[17] J.N. Ness, T.F. Page, Microstructural evolution in reaction-bonded silicon carbide, J Mater Sci. 21 (1986) 1377-1397
[18] V. Bougiouri, R. Voytovych, N. Rojo-Calderon, J. Narciso, N. Eustathopoulos, The Role of the Chemical Reaction in the Infiltration of Porous Carbon by NiSi Alloys, Scr. Mater. 54 (2006) 1875-1878.
[19] M. Caccia, S. Amore, D. Giuranno, R. Novakovic, E. Ricci, J. Narciso, Towards optimization of SiC/CoSi2 composite material manufacture via reactive infiltration: Wetting study of Si–Co alloys on carbon materials, J. Eur. Ceram. Soc. 35 (2015) 4099-4106.
[20] Y. Tong, S. Bai, Q.H. Qin, H. Zhang, Y. Ye, Effect of infiltration time on the microstructure and mechanical properties of C/C-SiC composite prepared by Si-Zr10 alloyed melt infiltration, Ceram. Inter. 41 (2015) 4014-4020.
[21] L. Hozer, Y.M. Chiang, Reactive-infiltration processing of SiC-metal and SiC-intermetallic composites, J. Mater. Sci. 11 (1995) 2346-2357.
[22] O. Dezellus, N. Eustathopoulos. Fundamental issues of reactive wetting by liquid metals. J Mater Sci. 45(2010) 4256-4264.
[23] D. Sergi, A. Camarano, J. M. Molina, A. Ortona, J. Narciso. Surface growth for molten silicon infiltration into carbon millimeter-sized channels: Lattice-Boltzmann simulations, experiments and models. Int. J. Mod. Phys. C. (2015), DOI: 10.1142/S0129183116500625
[24] M. Caccia, A. Camarano, D. Sergi, A. Ortona, J. Narciso (2015). Wetting and Navier-Stokes Equation - The Manufacture of Composite Materials. In: Dr. M. Aliofkhazraei (Ed.), Wetting and Wettability.
[25] N.R Calderon, M. Martínez-Escandell, J. Narciso, F. Rodríguez-Reinoso. The combined effect of porosity and reactivity of the carbon preforms on the properties of SiC produced by reactive infiltration with liquid Si. Carbon 47(2009) 2200-2210.
[26] V. Milekhine, M.I. Onsøien, J.K. Solberg, T. Skaland, Mechanical properties of FeSi (ε), $FeSi_2$ (ζα) and Mg_2Si, Intermetallics 10 (2002) 743-750.
[27] D.I. Anton, D.M. Shah, D.N. Duhl, A.F. Giamei, Selecting High-temperature structural intermetallic compounds: the engineering approach, JOM 41 (1989) 12-17.
[28] D.M Shah, D. Berczik, D. L. Anton, R. Hecht, Appraisal of other silicides as structural materials. Mater. Sci. Eng.: A. 155 (1992) 45-57.
[29] K. Maex, M. Van Rossum, Properties of Metal Silicies, Inspec, London, United Kingdom, 1995.
[30] P. J. Yunes Rubio, N. Saha-Chaudhury, L. Hong, R. Bush, V Sahajwalla, Dynamic Wetting of Graphite and SiC by Ferrosilicon Alloys and Silicon at 1550°C. ISIJ International, 46 (2006) 1570–1576.
[31] D. Zhu, M. Gao, H. Pan, Y. Liu, X. Wang, Y. Pan, F.J. Oliveira, J. M Vieira. Reactive infiltration processing of SiC/Fe–Si composites using preforms made of coked rice husks and SiC powder. Ceram. Inter. 39 (2013), 3831-3842.

[32] N. R. Calderon, R. Voytovych, J. Narciso, N. Eustathopoulos. Pressureless infiltration versus wetting in AlSi/graphite system. J Mater Sci. 45 (2010) 4345-4350.
[33] K. Landry, C. Rado, N. Eustathopoulos. Influence of Interfacial Reaction Rates on the Wetting Driving Force in Metal/Ceramic Systems, Metall. Mater. Trans. A. 27 (1996) 3181-3186.
[34] N.R. Calderon, R. Voytovych, J. Narciso, N. Eustathopoulos. Wetting dynamics versus interfacial reactivity of AlSi alloys on carbon. J Mater Sci. 45 (2010) 2150-2156.
[35] V. Bougiouri, R. Voytovych, O. Dezellus, N. Eustathopoulos. (2007). Wetting and reactivity in Ni–Si/C system: experiments versus model predictions. J Mater Sci. 42 (2007), 2016-2023.
[36] P. Greil, T. Lifka, A. Kaindl. (1998). Biomorphic cellular silicon carbide ceramics from wood: I. Processing and microstructure. J. Eur. Ceram. Soc. 18 (1998) 1961-1973.
[37] G. Amirthan, A. Udayakumar, V.B. Prasad, M. Balasubramanian. Synthesis and characterization of Si/SiC ceramics prepared using cotton fabric. Ceramics International, 35 (2009), 967-973.
[38] T. Xue, Z. J. W. Wang, Preparation of porous SiC ceramics from waste cotton linter by reactive liquid Si infiltration technique. Mater. Sci. Eng.: A. 527 (2010) 7294-7298.
[39] G. Hou, Z.J.J. Qian, Effect of holding time on the basic properties of biomorphic SiC ceramic derived from beech wood. Mater. Sci. Eng.: A. 452-453 (2007) 278-283.
[40] R. Arpón, J.M. Molina, R.A. Saravanan, C. García-Cordovilla, E. Louis, J. Narciso, Acta Mater. 51 (2003) 3145-3156.
[41] T. Etter, M. Papakyriacou, P. Schulz, P.J. Uggowitzer, Physical properties of graphite/aluminium composites produced by gas pressure infiltration method, Carbon 41 (2003) 1017-1024.

ANNEX A

In the present study twelve Si-Fe alloys were manufactured using 4 different concentrations (Si5wt.%Fe, Si15wt.%Fe, Si25wt.%Fe y Si35wt.%Fe). These alloys were in-house prepared using a mixture of high purity materials, Fe (Goodfellow, 99.95% purity) and Si (Petroceramics, 99.999% purity). The procedure to manufacture these alloys consisted in the following steps: (i) Crucibles manufacture. Crucibles were machined from 50 mm diameter bar of high density molded graphite, quality CB26, provided by Carbosystem. The graphite bar was sectioned in pieces with lengths of 100 mm and using a lathe, a hole of 85 mm of depth and 13 mm of diameter was made in the center of the bar. (ii) Crucibles were coated with boron nitride (BN) to prevent the reaction between carbon and the alloy. This coating consists in 3 layers of BN spray applied to the entire crucible inner surface followed by a heat treatment in Ar with a flow of 100 cm^3/min, using a heating rate of 5 °C/min until 1500 °C and a holding time of 30 minutes to guarantee the release of volatile compounds and the adherence of the coating layer to the crucible. Finally the coated crucible was cooled down until ambient temperature and through visual inspection it was checked that the coating was continuous. (iii) Alloying elements were molten inside the crucible, using Linn High Therm GmbH induction furnace, model MFG-15. Before melting, atmosphere was cleaned using three flushing steps alternating between vacuum (3-6 mbar) and high purity Argon. The main purpose of these flushing steps is to minimize the oxygen content in the furnace chamber to prevent the oxidation of the alloys. After this step, the system was heated, under Ar atmosphere (P = 0.15 MPa), over the melting point of the alloy during 20 minutes in order to achieve homogeneity in the melt. Finally the melt was cooled rapidly until ambient temperature.

Microstructure and element segregation were studied after alloy preparation. Firstly the ingots were removed from the crucible, followed by a surface cleaning with SiC grinding paper to remove the BN. After the surface cleaning, five millimeters from the top and bottom of the ingot were cut to eliminate oxide phases segregated during the melting. In order to evaluate the segregation during the cooling process a slice of alloy, with a thickness of 1 mm, was cut from the center of the ingot. This slice was divided in three pieces and studied independently. Fig. A1 shows a schematic representation of the sectioned ingot used to study this phenomenon.

In order to study the composition from the sectioned pieces, X-Ray fluorescence (XRF) was used. Table A1 shows the averaged compositions obtained in this analysis. According to these results, silicon and iron were the only elements in the alloy and no traces of BN were found. The value of Fe and Si concentration for the three different slices (top, middle and bottom) were averaged and standard deviation was calculated. Deviations from the average values are low, between 1.0-2.1 % indicating that segregation of alloying elements along the ingot is low.

Fig. A1. *Schematic representation of the sectioned ingot used to study element segregation.*

Table A1*- Metal content in alloys determined by XRF*

Alloys	***Nominal (% weight)***		***Experimental - XRF (% weight)***	
	Si	***Fe***	***Si***	***Fe %***
Si-5wt.%Fe	93.4	6.6	94.8 ± 0.95	4.2 ± 1.0
Si-15wt.%Fe	85.3	14.7	85.0 ± 1.7	13.3 ± 1.7
Si-25wt.%Fe	76.1	23.9	78.2 ± 1.3	20.5 ± 1.3
Si-35wt.%Fe	65.1	34.9	63.5 ± 2.1	34.4 ± 2.1

The microstructure of the alloys and phase composition were evaluated with optical microscopy (OM) and X-ray diffraction (XRD), respectively. Fig. 2 shows optical microscopy images of cross-sections of the different alloys with the corresponding XRD pattern. The OM images show the evolution of the alloy phases as the Fe content increases and the XRD patterns show the presence of two crystalline phases in the alloy, Si (cubic) and α-$FeSi_2$ (orthorhombic).

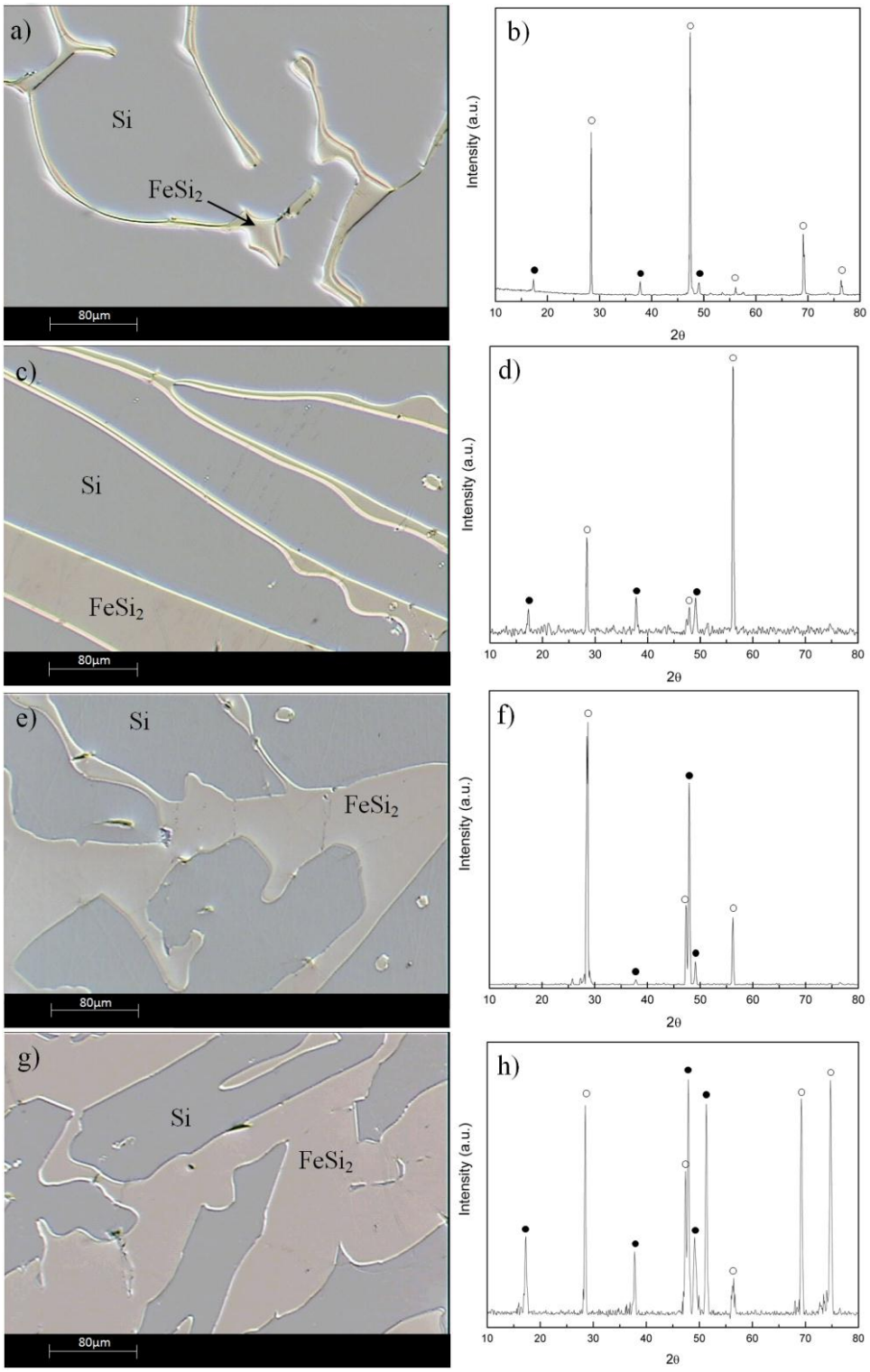

Fig. 2. *Optical microscopy images of cross-sections and X-ray diffractogram of alloys with a Fe content of 5 wt.% (a-b), 15 wt.% (c-d), 25 wt.% (e-f) and 35 wt.% (g-h). In the diffractograms, filled circles indicate the diffraction peaks of α-$FeSi_2$ and empty circles the diffraction peaks of Si.*